Available online at www.sciencedirect.com
ScienceDirect
Earth and Planetary Science Letters 261 (2007) 134–142
EPSL
www.elsevier.com/locate/epsl

The infrared signature of water associated with trivalent cations in olivine

Andrew J. Berry [a,*], Hugh St.C. O'Neill [b], Jörg Hermann [b], Dean R. Scott [b]

[a] Department of Earth Science and Engineering, Imperial College London, South Kensington, SW7 2AZ, United Kingdom
[b] Research School of Earth Sciences, Australian National University, Canberra, ACT 0200, Australia

Received 19 March 2007; received in revised form 14 June 2007; accepted 17 June 2007
Available online 23 June 2007
Editor: G.D. Price

Abstract

Forsterite crystals were synthesised under water saturated conditions at 1400 °C and 1.5 GPa doped with trace amounts of either B, Al, Sc, Ti, V, Cr, Mn, Fe, Co, Ga, Y, Zr, In, Sm, Gd, Dy, Tm, or Lu. The common and intense hydroxyl stretching bands in the infrared spectra of spinel peridotite olivine, at 3572 and 3525 cm^{-1}, were only reproduced in the presence of Ti. Those samples where the trace element substitutes as the trivalent cation on the Mg^{2+} site were identified from a systematic variation in concentration with the trivalent ionic radius. The hydroxyl region of all samples is essentially identical except for between 3300 and 3400 cm^{-1}. This region is characterised by one or more bands, with the energy of the most intense feature being correlated with the ionic radius of the trivalent cation. The integrated intensity of these hydroxyl bands also correlates with the concentration of the trivalent cation. These correlations provide unambiguous evidence that bands, or peaks, in this region correspond to water at defect sites associated with trivalent cations. "Trivalent peaks" are sometimes observed in samples of mantle olivine and most likely indicate water associated with Fe^{3+}. The water at this site is not incorporated under normal mantle conditions and should not be included in estimates of the water capacity of mantle olivine. These results emphasise the importance of identifying the infrared signature of different water substitution mechanisms.

Keywords: olivine; infrared spectroscopy; nominally anhydrous minerals; mantle water; experimental petrology; hydrated defects; trivalent trace elements

1. Introduction

Water in the Earth's mantle is believed to be stored as hydroxyl groups, OH, at defect sites in nominally anhydrous minerals (e.g. Bell and Rossman, 1992; Ingrin and Skogby, 2000). The presence of water strongly affects the geochemical and geophysical properties of the mantle and hence the amount, defect site, partitioning, and diffusion of hydrogen in mantle minerals has received considerable attention (Keppler and Smyth, 2006).

The hydroxyl region of the infrared absorption spectra of mantle olivines exhibits a complex and variable pattern of bands (Miller et al., 1987; Matsyuk and Langer, 2004). While the area under these bands can be used to quantify the amount of water (Paterson, 1982;

* Corresponding author.
E-mail address: a.berry@imperial.ac.uk (A.J. Berry).

0012-821X/$ - see front matter © 2007 Elsevier B.V. All rights reserved.
doi:10.1016/j.epsl.2007.06.021

Libowitzky and Rossman, 1997; Bell et al., 2003), information about the water site or sites contained in the energies and intensities of the bands is poorly understood. The defect sites occupied by hydroxyls must depend on the conditions of water incorporation. The assignment of infrared absorption bands may thus identify features that fingerprint or are diagnostic of various geological processes. This will allow water of a non-mantle or secondary origin (e.g. associated with serpentinisation or oxidation) to be recognised and hence excluded from estimates of the primary water content of mantle olivine.

Attempts to identify water sites in olivine have largely relied on relating the orientation of OH bonds, determined from polarised infrared experiments on oriented single crystals, to the crystal structure (Beran and Putnis, 1983; Libowitzky and Beran, 1995; Lemaire et al., 2004). There have also been attempts to use X-ray diffraction (Smyth et al., 2006) and to computationally relate the infrared vibrational energy and polarisation to models of defect sites (Brodholt and Refson, 2000; Braithwaite et al., 2003; Walker et al., 2007). An alternative approach is to synthesise olivine crystals under controlled experimental conditions to identify the factors that produce different absorption bands (Matveev et al., 2001; Lemaire et al., 2004; Berry et al., 2005). These synthesis experiments have all been undertaken at relatively modest pressures corresponding to the spinel peridotite facies of the mantle. It was found that bands near 3600 cm^{-1} (3612, 3579, and 3567 cm^{-1}) are produced at low silica activities (assigned to hydrated Si vacancies) and that bands at 3160 and 3220 cm^{-1} occur at high silica activities (hydrated Mg vacancies). Additionally, it was shown that the most common and intense stretching bands observed for spinel peridotite olivine (at 3572 and 3525 cm^{-1}) derive from water at defect sites associated with the trace element Ti (Berry et al., 2005). A series of experiments found that these bands could only be reproduced in olivines grown under upper mantle conditions from compositions containing Ti. The bands were attributed to a Ti–clinohumite-like point defect site. These assignments are all supported by computational studies in which the infrared polarisation of the lowest energy defect is consistent with that observed experimentally (Braithwaite et al., 2003; Walker et al., 2007). In contrast, Ti–clinohumite lamellae defects, which have been recognised previously, are characterised by a band near 3410 cm^{-1} (Kitamura et al., 1987; Risold et al., 2001; Hermann et al., 2007). Other bands at 3355 and 3325 cm^{-1} have been attributed to water associated with Fe^{3+} since they occur experimentally only in Fe-bearing compositions, in particular when oxidation is likely to have occurred (Berry et al., 2005). It has also been suggested that water is involved in a coupled substitution with Al in mantle olivine (Hauri et al., 2006). To test the possibility that various trace elements may be involved in hydroxyl substitutions we have investigated the effect of a large number of trivalent cations on the infrared spectrum of hydrous olivine.

2. Experimental

Crystals of forsterite were synthesised from reagent grade oxides under water saturated conditions, in Pt capsules, at 1400 °C and 1.5 GPa for 24 h using a salt/pyrex/MgO assembly in a piston-cylinder apparatus. An oxide composition corresponding to Mg_2SiO_4 + 10 wt.% SiO_2 + 7 wt.% H_2O + 1 wt.% of either M_2O_3 (where M = B, Al, Sc, Cr, Fe, Co, Ga, Y, In, Sm, Gd, Dy, Tm, Lu), TiO_2, V_2O_5, Mn_3O_4, or ZrO_2 was used in the experiments. These compositions are expected to produce olivine + melt + fluid (Kushiro et al., 1968). A reference sample, or blank, was also prepared. In some cases Re/ReO_2 or Ru/RuO_2 was added as a layer (~10 wt.%) at one end of the capsule to buffer the oxygen fugacity (fO_2) at $\log fO_2$ values relative to Ni/NiO (NNO) of NNO + 1.5 and NNO + 5 respectively (Pownceby and O'Neill, 1994; O'Neill and Nell, 1997). These buffers are never consumed due to their abundance relative to the dopant element and the small H_2 content of the fluid at these fO_2s. More oxidising conditions were achieved using a layer of PtO_2, which breaks down at the experimental conditions to Pt and O_2. The partial pressure of O_2 in the resulting O_2–H_2O–SiO_2 fluid at the confining pressure defines the fO_2, which will be extremely oxidised (~NNO + 9). Experiments with B, Al, Sc, Y, Sm, Gd, Dy, Tm, and Lu were unbuffered as only the trivalent oxidation state is expected. PtO_2 was added to the Ga and In experiments to prevent alloying with the Pt capsule, and to the Fe, Co, and Mn experiments to inhibit the formation of divalent cations, which will readily substitute into forsterite. V was buffered with Re/ReO_2 in an attempt to preferentially stabilise V^{3+} relative to V^{2+}, V^{4+}, or V^{5+}, while Re/ReO_2 and Ru/RuO_2 were both used for Cr to try and distinguish the effects of Cr^{2+}, Cr^{3+}, and Cr^{6+}. Experiments on Ti were both unbuffered and with added PtO_2.

The concentration of trace elements in forsterite was determined by laser ablation inductively coupled plasma mass spectrometry (LA-ICPMS) using a pulsed ArF (193 nm) excimer laser and an Agilent 7500 ICP-

MS. Individual crystals were mounted in epoxy for analysis. Laser sampling used a circular spot with a diameter of 110 μm, a 5 Hz ablation rate, and a laser pulse energy of 70 mJ, in an Ar–He atmosphere. Nist612 glass was used as the external standard with Si as the internal standard.

Infrared spectra were recorded using unpolarised light from unoriented single crystals with a Bruker A590 infrared microscope and Bruker IFS28 infrared spectrometer. This experiment optimises the probability of light being absorbed by all the hydroxyl groups in a sample and is ideal for identifying the number and energy of hydroxyl bands (the spectral fingerprint). Spectra were recorded for a number of crystals (>10) of different orientations (inferred from the Si–O overtone bands, which also distinguish olivine from orthopyroxene) and the results reported are representative of the average intensity distribution. Spectra were normalised to the integrated intensity of the Si–O stretching overtone modes between 1630 and 2100 cm^{-1} (Lemaire et al., 2004; Matveev et al., 2005). Water contents were estimated from the integrated intensity of the hydroxyl bands using the calibrations of Bell et al. (2003), Libowitzky and Rossman (1997), and Paterson (1982); the path length was approximated by referencing the area of the Si–O overtone modes to that of a randomly oriented sample prepared to a known thickness, and the results were multiplied by an orientation factor of three, which relates the total water content to the intensity obtained from unpolarised spectra of unoriented crystals (Sambridge et al., submitted for publication; Kovacs et al., submitted for publication).

3. Results

Fig. 1 shows an opened Pt capsule after an experiment. It contains loose forsterite crystals at the end that was adjacent to the thermocouple and a solid mass of quenched melt at the other. The loose crystals indicate that a fluid phase, in addition to the melt, was present at the experimental conditions, which were hence water saturated. The crystals vary in size between experiments from ~50–500 μm. Large numbers of large crystals were favoured by the use of long capsules and the resulting temperature gradient. The crystals were identified to be almost entirely forsterite from the Si–O stretching overtone bands (Matveev et al., 2005).

The concentration of the M^{n+} dopant in forsterite from each experiment is given in Table 1. The blank and impurity element concentrations are essentially negligible. The dopant concentrations as a function of the trivalent ionic radius are shown in Fig. 2. For those elements that are unambiguously trivalent, excluding the smallest cation, B, the concentrations vary smoothly and systematically around a maximum near the ionic radius of Mg^{2+}. This identifies substitution as the trivalent cation on one of the two octahedral sites occupied by Mg. As expected, the dopant with the highest concentration is Sc, the ionic radius of which is the closest to that of Mg^{2+}. Deviations from the trend, e.g. Cr, Mn, and Co (not shown), indicate substitution as other or additional oxidation states. For example, the Co-bearing crystals are deep pink, consistent with substitution as Co^{2+}.

Fig. 1. A Pt capsule, after an experiment, for which one side has been peeled back to reveal a mass of forsterite crystals and a slug of quenched hydrous melt.

The hydroxyl stretching region of the infrared absorption spectrum of each sample is shown in Fig. 3. In most cases the bands characteristic of high and low silica activities at these pressures, 3165 and 3612 cm^{-1} respectively, are both observed (Lemaire et al., 2004; Berry et al., 2005). Between samples, these bands are comparable in intensity, indicating that the normalisation procedure is not unreasonable. The high energy bands of the Ti-bearing sample are unique. The major spectral differences occur between 3300 and 3400 cm^{-1}. This region is characterised by an intense peak around 3350 cm^{-1}. For some elements several weaker peaks, at lower energy, are also observed. The energy of the most intense peak varies systematically with the trivalent ionic radius (Fig. 4). The integrated intensity (area) of the peaks or bands in this region varies with the trivalent ion

Table 1
Energy of infrared absorption bands between 3300 and 3400 cm^{-1} in order of decreasing intensity, and their integrated area, for forsterite containing the element indicated

Element	Sample	Buffer [a]	Ionic Radius (M^{3+}, pm) [b]	ppm (wt) [c]	Energy (cm^{-1}) [d]			Area [e]	H_2O (ppm) [f]	Notes [g]
B	c2171		27.0	42(4)						
Al	d530		53.5	52(5)	3344.5	3350.5	3322	33	18	
Sc	c2127		74.5	1726(73)	3356	3321		543	306	Ti(2), Mn(20)
Ti	c2079		67.0	384(5)	3350.5	3338.5	3312	36	20	Mn(15), Co(4)
Ti	c2174	PtO_2	67.0	70(2)						Fe(8)
Cr	c2148	Ru/RuO_2	61.5	1860(140)	3325.5	3354	3306	400	228	Fe(7), Ru(10)
Cr	c2152	Re/ReO_2	61.5	1960(100)	3325.5	3354	3306	470	266	Fe(5), Re(3)
V	c2190	Re/ReO_2	64.0	150(30)	3351	3348 [h]	3336	82	46	Re(19), Cr(6), Mn(5), Fe(60), Co(3)
Mn	c2189	PtO_2	64.5	2065(40)	3345	3350	3368	7	4	Fe(4)
Fe	c2134	PtO_2	64.5	408(20)	3350	3331	3309.5	75	42	
Co	c2140	PtO_2	61.0	5340(100)						Fe(5)
Ga	c2138	PtO_2	62.0	100(4)	3346	3334.5	3310	36	20	Sc(2), Fe(7)
Y	c2165		90.0	264(26)	3359			89	50	Ti(2), Mn(6)
Zr	c2156	PtO_2	– [i]	5(1)						Fe(3)
In	c2181	PtO_2	80.0	553(149)	3354	3308.5		96	54	Fe(5)
Sm	c2161		95.8	5(2)						
Gd	c2184		93.8	18(1)	3358.5			2	1	
Dy	c2183		91.2	50(8)	3358.5			17	10	
Tm	c2182		88.0	206(36)	3358.5			31	18	Lu(3)
Lu	d528		86.1	323(71)	3359			36	21	
blank	c2168									B(3–4), Cr(1–2), Mn(2–4)

[a] Oxygen fugacity buffer.
[b] Normalised to a thickness of 1 cm.
[c] Concentration of trace element impurities in ppm (by wt.); those listed for the blank are present in all samples. Pt varied markedly: 35(50) for the experiments with PtO_2, otherwise 20(30). All other impurities are <1 ppm.
[d] VI coordination (high spin) (Shannon, 1976).
[e] All uncertainties are one standard deviation.
[f] To nearest 0.5 cm^{-1}.
[g] ppm by wt. for trivalent bands using calibration from Bell et al. (2003); for discussion of uncertainties see text.
[h] Shoulder on peak at 3351 cm^{-1}.
[i] Zr^{4+}.

concentration (Fig. 5). For the Cr-bearing forsterites, the spectra and Cr concentrations were essentially identical for samples buffered with both Re/ReO_2 and Ru/RuO_2. The spectral data for these samples, and that for Mn, are anomalous and were omitted from the plots. The spectra of the two Ti-bearing samples were identical except for the presence of bands near 3350 cm^{-1} in the unbuffered experiment (shown in Fig. 3). Weak bands were also observed between 3400 and 3500 cm^{-1} in a number of experiments (e.g. In); these are at constant energies and are not discussed further.

4. Discussion

The hydroxyl region of the infrared absorption spectra of most samples (Fig. 3) exhibits bands at 3612, 3579, and 3567 cm^{-1}, attributed to hydrated Si vacancies (Matveev et al., 2001; Lemaire et al., 2004; Berry et al., 2005), plus a band at 3165 cm^{-1}, assigned to a hydrated Mg vacancy (Lemaire et al., 2004; Berry et al., 2005). The presence of both these low and high silica activity bands is consistent with the distribution of hydrated defects that is thermodynamically expected at the high silica and water activities of these experiments (Walker et al., 2007). The bands are not, however, observed in natural samples from the upper mantle equilibrated at similar pressures to these experiments (i.e. spinel peridotite facies), which are instead characterised by bands at 3572 and 3525 cm^{-1}. These "spinel peridotite" bands are only reproduced by the Ti-bearing experiment (Fig. 3). Other tetravalent cations (e.g. Zr) have no effect on the spectra, suggesting a unique role for Ti^{4+} in the incorporation of water in spinel peridotite olivine. This Ti-related spectral fingerprint has been assigned to a Ti–clinohumite-like point defect (Berry et al., 2005).

The energy of the most intense infrared absorption peak between 3300 and 3400 cm^{-1} exhibits a

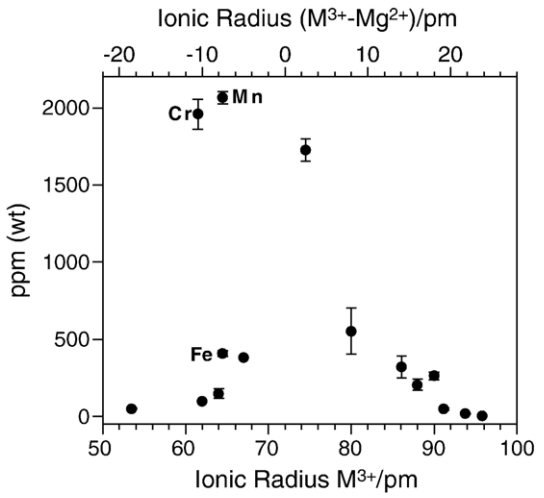

Fig. 2. Concentration (ppm by weight) of dopant elements in forsterite as a function of the trivalent (M^{3+}) ionic radius. (M^{3+}–Mg^{2+}) is the difference between the size of the trivalent cation and Mg^{2+}. Error bars are one standard deviation of the analytical precision.

remarkable correlation with the trivalent ionic radius of the substituting element (Fig. 4). Additionally, the integrated intensity of the bands in this region varies with the concentration of the trivalent cation (Fig. 5a). As might be expected, no peak is observed for the Co-bearing sample, since the anomalously high concentration and colour indicate substitution as Co^{2+}. Similarly, only weak peaks were found for the Mn-doped sample, where substitution predominantly as Mn^{2+} seems to have occurred. Bands in this region were observed for the unbuffered Ti sample, synthesised under the mildly reducing conditions intrinsic to the apparatus, but are absent under the strongly oxidising conditions of the experiment with PtO_2, where only Ti^{4+} is expected. Peaks were also not observed for the B-bearing sample, where due to the small size of the cation substitution is expected on the tetrahedral site; the absence of any additional hydroxyl bands indicates that the substitution $B^{3+}+H^{+}\leftrightarrow Si^{4+}$ is not important (Kent and Rossman, 2002). Taken together these results provide unambiguous evidence that the peaks between 3300 and 3400 cm^{-1} are due to water associated with a trivalent cation. Peaks in this region attributed to water associated with Al^{3+} have also been reported by Grant et al. (in press). The spectral range over which these "trivalent peaks" occur will hereafter be referred to as the "trivalent region".

The correlation between the peak energy and ionic radius exhibits some scatter (Fig. 4). This is not unexpected since in addition to the size of the trivalent cation, the nature of its bonding (e.g. degree of

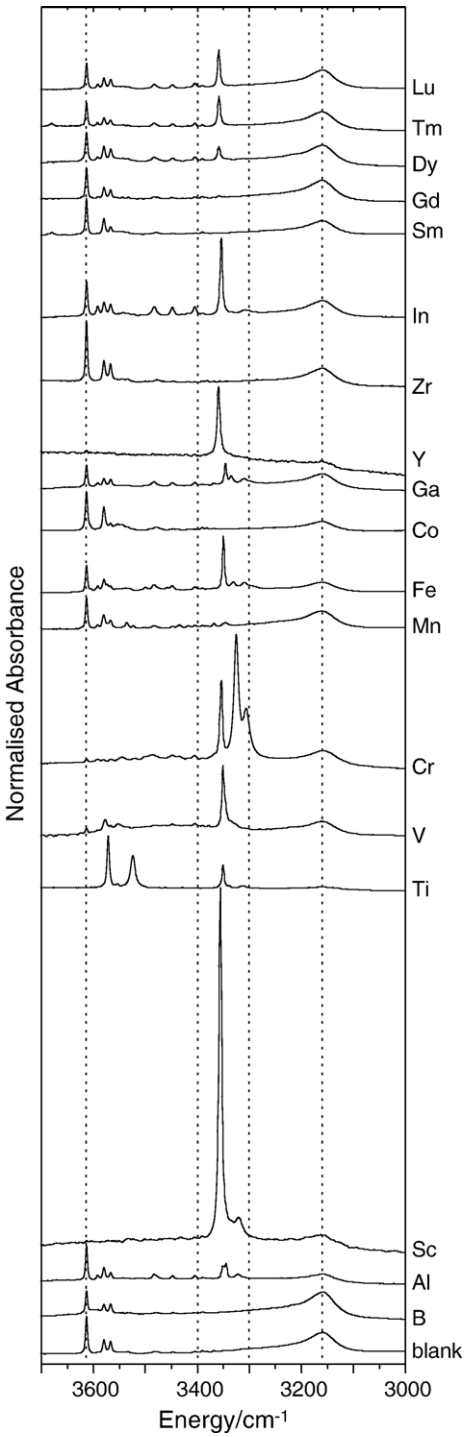

Fig. 3. OH stretching region of infrared absorption spectra of forsterite doped with the elements indicated. The dashed lines at 3612 and 3165 cm^{-1} indicate the low and high silica activity bands, while those at 3400 and 3300 cm^{-1} indicate the spectral region characterised by bands attributable to the trivalent dopant element. Spectra were recorded from unoriented single crystals using unpolarised light and were normalised to the integrated intensity of the Si–O stretching overtone bands. Spectra are offset for clarity.

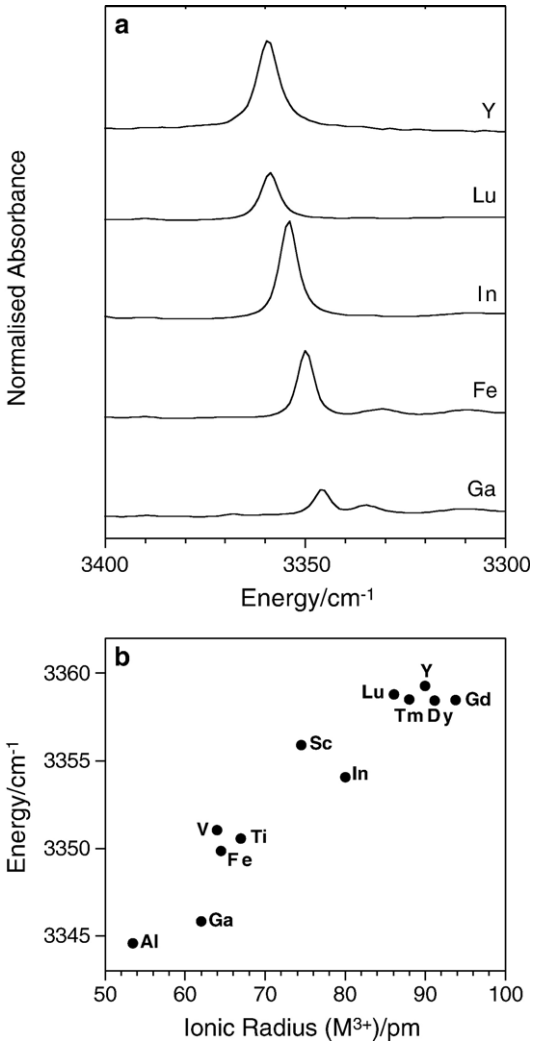

Fig. 4. (a) Trivalent region of the infrared absorption spectra of forsterite doped with the elements indicated, and (b) the energy of the most intense peak in this region as a function of the trivalent ionic radius; the error in relative energy is equal to the size of the point.

covalency) may affect the hydroxyl vibrational energy. For the largest ionic radii (Y and REEs) the peak energy is approximately constant indicating some sort of limit to the response of the structure to the coupled substitution.

The olivine structure contains two Mg sites, M1 and M2, and one Si. Taken together, partitioning and computational results suggest that most trivalent cations

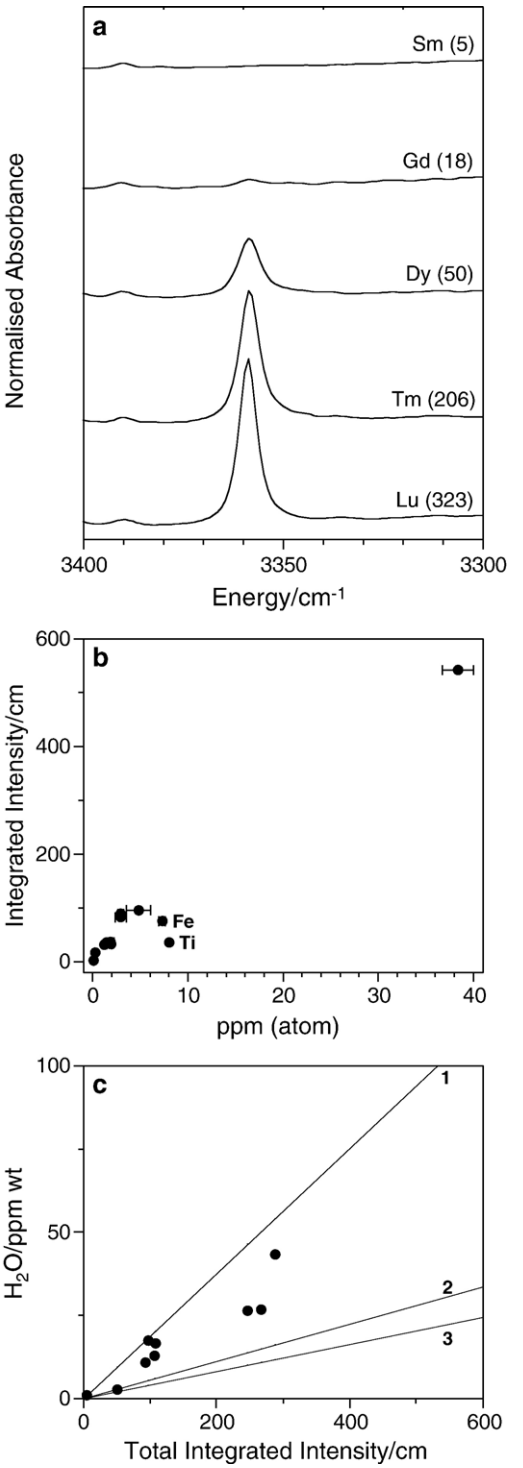

Fig. 5. (a) Trivalent region of the infrared absorption spectra of forsterite doped with the rare-earth elements indicated; the concentration (ppm by wt) is given in parenthesis, (b) the integrated intensity, normalised to 1 cm, of bands in the trivalent region as a function of the dopant concentration in ppm by atom, and (c) the amount of H_2O calculated from the trivalent cation concentration, assuming a 1:1 substitution mechanism, as a function of the total integrated trivalent band intensity (solid symbols). The calibrations of (1) Bell et al. (2003), (2) Libowitzky and Rossman (1997), and (3) Paterson (1982), are given by the solid lines. The data for Fe, Ti, and Sc have been omitted.

occupy the larger M2 site, charge balanced by either a M1 vacancy or the coupled substitution of Li^{+}(or Na^{+}) on M1, or Al^{3+} for Si^{4+} (Colson et al., 1989; Nielsen et al., 1992; Beattie, 1994; Purton et al., 1997; Richmond and Brodholdt, 2000). There is also evidence that small trivalent cations may substitute onto the M1 and Si sites (Rager, 1977; Gaite and Hafner, 1984; Gaite and Rager, 1997). In the present case, the relationship between concentration, the trivalent ionic radius, and the radius of Mg^{2+} (Fig. 2) is consistent with substitution on a Mg site. The correlation between the hydroxyl peak energy and the trivalent ionic radius (Fig. 4) indicates that the M^{3+} and H^{+} defects are associated, suggesting a coupled substitution of the form $H^{+}+M^{3+}\leftrightarrow 2\ Mg^{2+}$; for example, M^{3+} on M2 and H^{+} associated with a M1 vacancy. This is an M^{3+} incorporation mechanism additional to that available in an anhydrous system. A possible arrangement is for M^{3+} and H^{+} to occupy adjacent edge-sharing octahedra; M2 shares an edge with M1, while M1 shares edges with both M1 and M2. In this case only a single H^{+} site is available for the substitution of large trivalent cations on M2, but two H^{+} sites may be associated with small cations on M1. Thus, for substitution on both the M1 and M2 sites, up to three hydroxyl bands might be expected. Such a scenario is consistent with the spectral results in that only a single hydroxyl band is associated with the larger trivalent cations, such as Y and the REEs (M^{3+} on M2), but one intense (M^{3+} on M2) and two weaker (M^{3+} on M1) bands are observed for small cations (e.g. Al, Ga, Fe). This explanation of the variable number of bands in the trivalent region, however, is speculative and atomistic calculations similar to those reported recently for other substitution mechanisms are required to be definitive (Walker et al., 2007; Berry et al., in press). There is no evidence for the coupled substitution of H^{+} and small M^{3+} for Si^{4+} since the hydroxyl energy of such a defect is likely to differ significantly from the trend shown in Fig. 4b.

The integrated intensity of the trivalent bands is strongly correlated with the concentration of the trivalent dopant. This is illustrated for the rare-earth elements in Fig. 5a, where the intensity systematically decreases with decreasing concentration, disappearing into the noise for Sm. The integrated intensity of all the trivalent bands (since the multiplicity of bands is assumed to derive from various coupled substitutions) as a function of the dopant atomic concentration is shown in Fig. 5b. The obvious exceptions to an approximately linear correlation are the Fe-and Ti-bearing samples, both of which contain substitutions as additional oxidation states (Fe^{2+} and Ti^{4+}). Accordingly, the trivalent concentration is overestimated, which if corrected would result in a shift of the Fe and Ti points towards the general trend. The point for Sc may also deviate from the trend due to the possible contribution of an additional, non-hydrous, incorporation mechanism ($2Sc^{3+}+V_{Mg}\leftrightarrow 3\ Mg^{2+}$ (Colson et al., 1989; Nielsen et al., 1992)) to the total Sc content. Differences in the water activity due to the varied use of buffers may also affect the forsterite water content. In particular, the substantial fraction of O_2 in the fluid phase of the experiments with PtO_2 will reduce fH_2O by dilution. However, any effect is apparently of second order importance given that these samples do not deviate from the correlation between trivalent band intensity and trivalent element abundance defined by the combined set of experiments.

The amount of water associated with the trivalent bands was estimated for each sample from the concentration of the trivalent cation, assuming a 1:1 substitution. This amount as a function of the total integrated intensity is shown in Fig. 5c. Also shown are the amounts of water calculated from the total intensity using the Bell et al. (2003), Libowitzky and Rossman (1997), and Paterson (1982) calibrations. The results using Bell et al. are also given in Table 1. There are a number of sources of error contributing to the integrated intensity determination. Firstly, the thickness estimate contains relative errors between samples due to the effect of orientation on the Si–O overtone band intensities, and an absolute error due to referencing to a single sample. Secondly, as the spectra were acquired from unoriented crystals using unpolarised light an orientation factor is required to account for hydroxyl groups that were not excited in the experiment (Paterson, 1982). This factor is three, however, a large number of spectra (>10) are required for this method to give an accurate total integrated intensity (Sambridge et al., submitted for publication; Kovacs et al., submitted for publication). As a result, large and uncertain errors may be expected for the quoted values, however, it is emphasised that the aim of the present study is the determination of spectral signatures rather than quantification. Nevertheless, the expected water contents are nicely bracketed by the various literature calibrations, supporting the proposed coupled substitution. Given the likely errors, it is not possible to infer which, if any, of the existing calibrations may be appropriate for trivalent absorption bands.

Trivalent peaks are occasionally observed in natural and experimental samples (Miller et al., 1987; Bai and Kohlstedt, 1993; Zhao et al., 2004; Matsyuk and Langer, 2004; Matveev et al., 2005; Peslier and Luhr, 2006). The bands in natural olivine are broader than those reported

here (possibly due to local variations in the distribution of Mg and Fe around the substitutional site) and thus the resolution does not allow the cation with which the water is associated to be identified. Further, due to the larger lattice parameter of Fe-containing olivine relative to forsterite the vibrational energies are likely to differ. For example, the most intense band that appears to be associated with Fe^{3+} in mantle olivine occurs at 3325 cm^{-1} (Berry et al., 2005), compared with 3350 cm^{-1} for forsterite in this study. The anomalous trivalent band energies of the Cr-and Mn-bearing samples may be explained similarly as being due to the variation in lattice parameter arising from the large amount of substitution as the divalent cation. Nevertheless, it would seem that the most likely trivalent cation with which water is associated in natural olivines is Fe^{3+}; in annealing experiments the trivalent peaks increase in intensity with increasing temperature (Zhao et al., 2004), and the bands are observed in samples from evolved magmas where high Fe^{3+} contents might be expected (Matveev et al., 2005).

Ion probe measurements of water partitioning between olivine and melt in experimental samples have suggested a correlation between H^+ and Al^{3+} (Hauri et al., 2006). This coupled substitution was determined to be important at pressures up to 2 GPa. However, the absence of intensity in the trivalent region for the majority of natural spinel peridotite samples, or only minor contributions, indicates that such a substitution can not be a primary mechanism of water incorporation. This has also been noted by Grant et al. (in press). Further, the absence of any additional hydroxyl bands that are specific to the Al-doped sample indicates that there is no alternative substitutional mechanism for the enhanced incorporation of H in the presence of Al.

This work contributes to our understanding of the origin of hydroxyl bands in the infrared spectra of mantle olivine. Peaks between 3300 and 3400 cm^{-1} are due to water associated with trivalent cations, the most likely of which is Fe^{3+}. The relative paucity of these peaks in natural olivines suggests that this substitution mechanism is not typical for the mantle. Instead, these bands are diagnostic of an oxidising environment, which may be an anomalously oxidised source in a heterogeneous mantle, or more likely, a late-stage process associated with exhumation. For example, the absence of any correlation between the appearance of these bands in olivine from spinel peridotite xenoliths and the inferred oxidation state of the peridotite, as calculated from olivine–orthopyroxene–spinel oxygen geobarometry (Peslier and Luhr, 2006), indicates that they are not a primary mantle signature. Water incorporated by this mechanism is hence unlikely to represent "normal" mantle conditions and should not be included in models of olivine water capacity or mantle water content (Zhao et al., 2004). We also emphasise the importance of recognising the defect site or sites at which water is incorporated when attempting any experiments on the physical properties of hydrous olivine.

Acknowledgements

We thank Simon Kohn and an anonymous reviewer for their comments on the manuscript and the Australian Research Council for financial support.

References

Bai, Q., Kohlstedt, D.L., 1993. Effects of chemical environment on the solubility and incorporation mechanism for hydrogen in olivine. Physics and Chemistry of Minerals 19, 460–471.

Beattie, P., 1994. Systematics and energetics of trace-element partitioning between olivine and silicate melts: implications for the nature of mineral/melt partitioning. Chemical Geology 117, 57–71.

Bell, D.R., Rossman, G.R., 1992. Water in Earth's mantle: the role of nominally anhydrous minerals. Science 255, 1391–1397.

Bell, D.R., Rossman, G.R., Maldener, J., Endisch, D., Rauch, F., 2003. Hydroxide in olivine: a quantitative determination of the absolute amount and calibration of the IR spectrum. Journal of Geophysical Research 108, 2105. doi:10.1029/2001JB000679.

Beran, A., Putnis, A., 1983. A model of the OH positions in olivine, derived from infrared spectroscopic investigations. Physics and Chemistry of Minerals 9, 57–60.

Berry, A.J., Hermann, J., O'Neill, H.St.C., Foran, G.J., 2005. Fingerprinting the water site in mantle olivine. Geology 33, 869–872.

Berry, A.J., Walker, A.M., Hermann, J., O'Neill, H.St.C., Foran, G.J., Gale, J.D., in press. Titanium substitution mechanisms in forsterite. Chemical Geology. doi:10.1016/j.chemgeo.2007.03.010.

Braithwaite, J.S., Wright, K., Catlow, C.R.A., 2003. A theoretical study of the energetics and IR frequencies of hydroxyl defects in forsterite. Journal of Geophysical Research 108, 2284. doi:10.1029/2002JB002126.

Brodholt, J.P., Refson, K., 2000. An ab initio study of hydrogen in forsterite and a possible mechanism for hydrolytic weakening. Journal of Geophysical Research 105, 18977–18982.

Colson, R.O., McKay, G.A., Taylor, L.A., 1989. Charge balancing of trivalent trace elements in olivine and low-Ca pyroxene: a test using experimental partitioning data. Geochimica et Cosmochimica Acta 53, 643–648.

Gaite, J.M., Hafner, S.S., 1984. Environment of Fe^{3+} at the M2 and Si sites of forsterite obtained from EPR. Journal of Chemical Physics 80, 2747–2751.

Gaite, J.M., Rager, H., 1997. Electron paramagnetic resonance study of Fe^{3+} at M1 position in forsterite. Journal of Physics Condensed Matter 9, 10033–10039.

Grant, K.J., Kohn, S.C., Brooker, R.A., in press. The partitioning of water between olivine, orthopyroxene and melt synthesised in the system albite–forsterite–H_2O. Earth and Planetary Science Letters.

Hauri, E.H., Gaetani, G., Green, T.H., 2006. Partitioning of water during melting of the Earth's upper mantle at H_2O undersaturated conditions. Earth and Planetary Science Letters 248, 715–734.

Hermann, J., Fitz Gerald, J., Malaspina, N., Berry, A.J., Scambelluri, M., 2007. OH-bearing planar defects in olivine produced by the

breakdown of Ti-rich humite minerals from Dabie Shan (China). Contributions to Mineralogy and Petrology 153, 417–428.

Ingrin, J., Skogby, H., 2000. Hydrogen in nominally anhydrous upper-mantle minerals: concentration levels and implications. European Journal of Mineralogy 12, 543–570.

Kent, A.J.R., Rossman, G.R., 2002. Hydrogen, lithium, and boron in mantle-derived olivine: the role of coupled substitutions. American Mineralogist 87, 1432–1436.

Keppler, H., Smyth, J.R. (Eds.), 2006. Water in nominally anhydrous minerals, Reviews in Mineralogy and Geochemistry, vol. 62. Mineralogical Society of America. 478 pp.

Kitamura, M., Kondoh, S., Morimoto, N., Miller, G.H., Rossman, G.R., Putnis, A., 1987. Planar OH-bearing defects in mantle olivine. Nature 328, 143–145.

Kovacs, I.J., Hermann, J., O'Neill, H.St.C., FitzGerald, J., Sambridge, M., Horvath, G., submitted for publication. Quantitative absorbance spectroscopy with unpolarised light. Part II: Experimental evaluation and development of a protocol for quantitative analysis of mineral IR data. American Mineralogist.

Kushiro, I., Yoder Jr., H.S., Nishikawa, M., 1968. Effect of water on the melting of enstatite. Geological Society of America Bulletin 79, 1685–1692.

Lemaire, C., Kohn, S.C., Brooker, R.A., 2004. The effect of silica activity on the incorporation mechanism of water in synthetic forsterite: a polarised infrared spectroscopic study. Contributions to Mineralogy and Petrology 147, 48–57.

Libowitzky, E., Beran, A., 1995. OH defects in forsterite. Physics and Chemistry of Minerals 22, 387–392.

Libowitzky, E., Rossman, G.R., 1997. An IR absorption calibration for water in minerals. American Mineralogist 82, 1111–1115.

Matsyuk, S.S., Langer, K., 2004. Hydroxyl in olivines from mantle xenoliths in kimberlites of the Siberian platform. Contributions to Mineralogy and Petrology 147, 413–437.

Matveev, S., O'Neill, H.St.C., Ballhaus, C., Taylor, W.R., Green, D.H., 2001. Effect of silica activity on OH-IR spectra of olivine: implications for low-$a$$SiO_2$ mantle metasomatism. Journal of Petrology 42, 721–729.

Matveev, S., Portnyagin, M., Ballhaus, C., Brooker, R., Geiger, C.A., 2005. FTIR spectrum of phenocryst olivine as an indicator of silica saturation in magmas. Journal of Petrology 46, 603–614.

Miller, G.H., Rossman, G.R., Harlow, G.E., 1987. The natural occurrence of hydroxide in olivine. Physics and Chemistry of Minerals. 14, 461–472.

Nielsen, R.L., Gallahan, W.E., Newberger, F., 1992. Experimentally determined mineral-melt partition coefficients for Sc, Y and REE for olivine, orthopyroxene, pigeonite, magnetite and ilmenite. Contributions to Mineralogy and Petrology 110, 488–499.

O'Neill, H.St.C., Nell, J., 1997. Gibbs free energies of formation of RuO_2, IrO_2, and OsO_2: a high temperature electrochemical and calorimetric study. Geochimica et Cosmochimica Acta 61, 5279–5293.

Paterson, M.S., 1982. The determination of hydroxyl by infrared absorption in quartz, silicate glasses and similar materials. Bulletin Mineralogie 105, 20–29.

Peslier, A.H., Luhr, J.F., 2006. Hydrogen loss from olivines in mantle xenoliths from Simcoe (USA) and Mexico: mafic alkalic magma ascent rates and water budget of the sub-continental lithosphere. Earth and Planetary Science Letters 242, 302–319.

Pownceby, M.I., O'Neill, H.St.C., 1994. Thermodynamic data from redox reactions at high temperatures. IV. The Re–ReO_2 oxygen buffer: an experimental calibration using emf and hydrothermal methods. Contributions to Mineralogy and Petrology 118, 130–137.

Purton, J.A., Allan, N.L., Blundy, J.D., 1997. Calculated solution energies of heterovalent cations in forsterite and diopside: implications for trace element partitioning. Geochimica et Cosmochimica Acta 61, 3927–3936.

Rager, H., 1977. Electron spin resonance of trivalent chromium in forsterite, Mg_2SiO_4. Physics and Chemistry of Minerals 1, 371–378.

Richmond, N.C., Brodholdt, J.P., 2000. Incorporation of Fe^{3+} into forsterite and wadsleyite. American Mineralogist 85, 1155–1158.

Risold, A.C., Trommsdorff, V., Grobéty, B., 2001. Genesis of ilmenite rods and palisades along humite-type defects in olivine from Alpe Arami. Contributions to Mineralogy and Petrology 140, 619–628.

Sambridge, M., FitzGerald, J., Kovacs, I.J., O'Neill, H.St.C., Hermann, J., submitted for publication. Quantitative absorbance spectroscopy with unpolarised light. Part 1: Theoretical development. American Mineralogist.

Shannon, R.D., 1976. Revised effective ionic radii and systematic studies of interatomic distances in halides and chalcogenides. Acta Crystallographica A32, 751–767.

Smyth, J.R., Frost, D.J., Nestola, F., Holl, C.M., Bromiley, G., 2006. Olivine hydration in the deep upper mantle: effects of temperature and silica activity. Geophysical Research Letters 33, L15301. doi:10.1029/2006GL026194.

Walker, A.M., Hermann, J., Berry, A.J., O'Neill, H.St.C., 2007. Three water sites in upper mantle olivine and the role of titanium in the water weakening mechanism. Journal of Geophysical Research 112, B05211. doi:10.1029/2006JB004620.

Zhao, Y., Ginsberg, S.B., Kohlstedt, D.L., 2004. Solubility of hydrogen in olivine: dependence on temperature and iron content. Contributions to Mineralogy and Petrology 147, 155–161.